PHASE SEPARATION

# Phospho-dependent phase separation of FMRP and CAPRIN1 recapitulates regulation of translation and deadenylation

Tae Hun Kim[1,2,3,4]*, Brian Tsang[1,2]*, Robert M. Vernon[1], Nahum Sonenberg[5,6], Lewis E. Kay[1,2,3,4], Julie D. Forman-Kay[1,2]†

**Membraneless organelles involved in RNA processing are biomolecular condensates assembled by phase separation. Despite the important role of intrinsically disordered protein regions (IDRs), the specific interactions underlying IDR phase separation and its functional consequences remain elusive. To address these questions, we used minimal condensates formed from the C-terminal disordered regions of two interacting translational regulators, FMRP and CAPRIN1. Nuclear magnetic resonance spectroscopy of FMRP-CAPRIN1 condensates revealed interactions involving arginine-rich and aromatic-rich regions. We found that different FMRP serine/threonine and CAPRIN1 tyrosine phosphorylation patterns control phase separation propensity with RNA, including subcompartmentalization, and tune deadenylation and translation rates in vitro. The resulting evidence for residue-specific interactions underlying co–phase separation, phosphorylation-modulated condensate architecture, and enzymatic activity within condensates has implications for how the integration of signaling pathways controls RNA processing and translation.**

Cells organize many biological processes by means of biomolecular condensates, including membraneless RNA-protein assemblies (*1*, *2*). Multivalent interactions drive the formation of condensates through phase separation, often associated with low-complexity intrinsically disordered protein regions (IDRs) within RNA-binding proteins (*1*, *2*). Moreover, posttranslational modifications (PTMs) within these disordered regions can control condensate assembly and disassembly as well as fundamental cellular processes occurring within condensates, including translational regulation (*1*, *2*). Mechanistically, translational regulation is linked to shortening of mRNA poly(A) tails by the CCR4-NOT complex, which is thought to repress translation by impeding ribosomal recruitment and initiating mRNA degradation (*3*). Supporting this mechanism, translational activation and deadenylation rates are observed to have an inverse relationship, with low translation and high deadenylation rates leading to short poly(A) tails and vice versa (*4*, *5*). However, the means by which deadenylation and translation are organized and coordinated within condensates remain enigmatic.

Many cytoplasmic condensates are involved in translational regulation, including stress granules, P-bodies, and neuronal granules (*6*–*8*). These condensates share a common set of protein components that are enriched for PTMs (*9*, *10*), which is suggestive of shared mechanisms of translational regulation. Two highly expressed RNA-binding proteins colocalized in many common cytoplasmic condensates are FMRP (fragile X mental retardation protein) and CAPRIN1 (fig. S1) (*10*–*12*). Both proteins are functionally involved in mRNA stability and translational repression (*13*–*15*) and are biologically linked to pathways involved in synaptic plasticity (*16*–*18*). Previously, phosphorylation-dependent phase separation of the isolated low-complexity region of FMRP was shown to be sufficient to inhibit in vitro translation, with implications for a general role of phase separation in regulating the activity-dependent translation that underlies learning and memory formation (*18*). Despite growing evidence for the functional importance of condensates (*19*, *20*) and the critical role of IDRs in phase separation (*1*, *2*), it remains challenging to directly examine transient PTM-dependent IDR interactions driving condensate formation and the regulation of biochemical processes (including deadenylation and translation) occurring within them.

To address these questions, we first reconstituted a model biomolecular condensate containing the intrinsically disordered C-terminal regions of FMRP (445–632, hereafter referred to as FMRP) and CAPRIN1 (607–709, hereafter referred to as CAPRIN1) for biophysical studies (Fig. 1A). Because previous studies have shown that these isolated disordered regions, individually, are important or sufficient for phase separation or granule formation (*15*, *18*, *21*), we hypothesized that these regions likely mediate FMRP-CAPRIN1 interactions and co–phase separation (fig. S2 and supplementary text). Using isothermal titration calorimetry (ITC), we detected no FMRP-CAPRIN1 interaction; however, after in vitro phosphorylation of FMRP (pFMRP; fig. S3, A and B) by casein kinase II (CK2), a known kinase that Ser/Thr-phosphorylates FMRP in vivo (*22*, *23*), we observed an effective 1 μM CAPRIN1-pFMRP binding affinity (fig. S4, A and B). Fluorescence resonance energy transfer (FRET) experiments between highly phosphorylated Cy3-labeled pFMRP and Cy5-labeled CAPRIN1 yielded an apparent 6 μM binding affinity, with decreasing affinities corresponding to lower

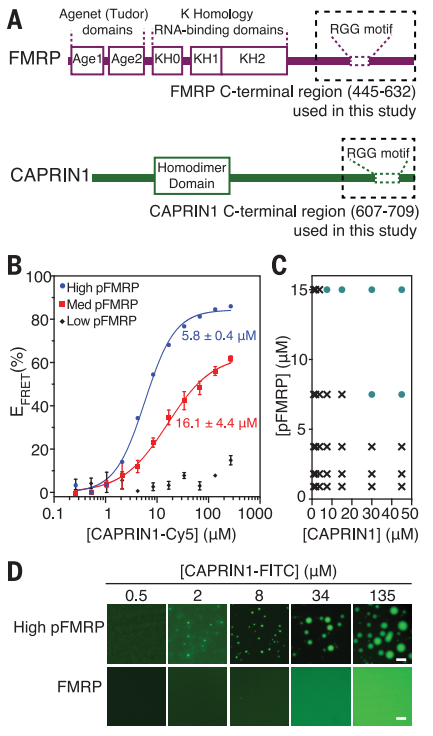


**Fig. 1. FMRP interacts with CAPRIN1 in a phosphorylation-dependent manner leading to co–phase separation.** (**A**) Schematic diagram of FMRP and CAPRIN1 showing the low-complexity regions used in this study (boxed). (**B**) FRET efficiencies measured between Cy3-labeled FMRP and Cy5-labeled CAPRIN1. CAPRIN1 binds pFMRP with a medium (~5) and high (~9) number of phosphorylation sites with apparent affinities of 16.1 ± 4.4 μM and 5.8 ± 0.4 μM, respectively. Error bars denote SD. (**C**) Phase diagram for co–phase separation of pFMRP and CAPRIN1. Teal dots represent conditions with observable droplet formation. (**D**) Fluorescence images of 10 μM pFMRP with increasing CAPRIN1-Cy5 concentrations. Scale bar, 4.8 μm.

[1]Program in Molecular Medicine, Hospital for Sick Children, Toronto, Ontario M5G 0A4, Canada. [2]Department of Biochemistry, University of Toronto, Toronto, Ontario M5S 1A8, Canada. [3]Department of Molecular Genetics, University of Toronto, Toronto, Ontario M5S 1A8, Canada. [4]Department of Chemistry, University of Toronto, Toronto, Ontario M5S 1A8, Canada. [5]Department of Biochemistry, McGill University, Montreal, Quebec H3G 1Y6, Canada. [6]Goodman Cancer Research Centre, McGill University, Montreal, Quebec H3A 1A3, Canada.
*These authors contributed equally to this work.
†Corresponding author. Email: forman@sickkids.ca

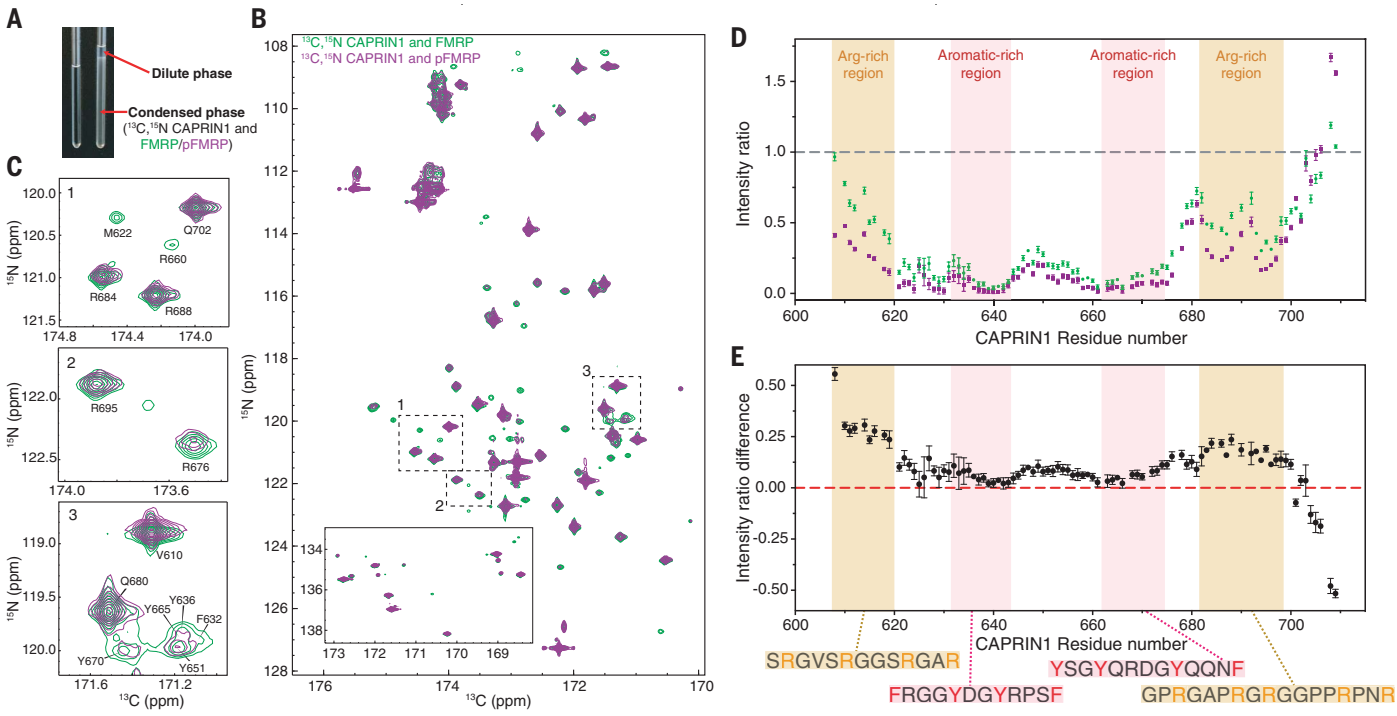


**Fig. 2. Solution-state NMR spectra of [$^{13}$C,$^{15}$N]CAPRIN1 in FMRP or pFMRP condensed phases.** (**A**) Images of [$^{13}$C,$^{15}$N]CAPRIN1 NMR samples in buffer (left) and FMRP condensed phase (right). (**B**) Overlay of CON spectra of [$^{13}$C,$^{15}$N]CAPRIN1 in FMRP (green) or in pFMRP (purple) condensed phases. (**C**) Examples of reduced intensities or small CSPs of arginine (1, 2) and aromatic (3) residues from the CON spectra. (**D**) Intensity ratio profiles of [$^{13}$C,$^{15}$N] CAPRIN1 in FMRP (green) and in pFMRP (purple) condensed phases after dividing by peak intensities from [$^{13}$C,$^{15}$N]CAPRIN1 in buffer and correcting for [$^{13}$C,$^{15}$N]CAPRIN1 concentrations (see supplementary materials). Beige shading highlights Arg-rich regions in CAPRIN1 exhibiting lower peak intensities in pFMRP versus FMRP condensed phase. Pink shading highlights CAPRIN1 aromatic-rich regions that exhibit sharply reduced peak intensities in both condensed phases relative to the dilute sample. The residue numbers correspond to the N atom of CON resonances. (**E**) Intensity ratio difference between the profiles in (D). Corresponding CAPRIN1 amino acid sequences of Arg-rich (beige) and aromatic-rich (pink) regions are shown below. Error bars are calculated based on the signal-to-noise ratios. Abbreviations: A, Ala; D, Asp; F, Phe; G, Gly; M, Met; N, Asn; P, Pro; Q, Gln; R, Arg; S, Ser; V, Val; Y, Tyr.

numbers of phosphate groups on pFMRP (Fig. 1B and fig. S3). Using fluorescence microscopy, we observed that CAPRIN1 does not co–phase-separate with FMRP (fig. S4, C to E) even at protein concentrations of 1 mM, but does so with pFMRP over a wide range of concentrations (Fig. 1, C and D, and fig. S4D). Because both FMRP and CAPRIN1 contain positively charged Arg-rich regions (Fig. 1A), we infer that FMRP phosphorylation reduces electrostatic repulsion to regulate its interaction and its ability to co–phase-separate with CAPRIN1.

To identify residues mediating pFMRP-CAPRIN1 interactions, we used nuclear magnetic resonance (NMR) spectroscopy and assigned the CAPRIN1 resonances (fig. S5). Titrating pFMRP into [$^{15}$N]CAPRIN1 resulted in co–phase separation, forming a turbid mixture containing many small droplets. Our results show global decreases in [$^{15}$N]CAPRIN1 amide peak intensities with no sizable chemical shift perturbations (CSPs) (fig. S6). This result is likely due to the slowed tumbling of partitioned [$^{15}$N]CAPRIN1 inside pFMRP-CAPRIN1 droplets reducing the signal and no detectable effects of CAPRIN1-pFMRP interactions outside of droplets in the dilute phase. Thus, binding and phase separation occur in tandem; this inference is further supported by monophasic ITC isotherms of CAPRIN1-pFMRP showing heat release only upon droplet formation (fig. S4).

To use NMR spectroscopy as a probe of interactions within condensates (*24*, *25*), we generated a single large condensed phase containing co–phase-separated [$^{13}$C,$^{15}$N]CAPRIN1 and pFMRP (Fig. 2A). Because CAPRIN1 and FMRP do not co–phase-separate (fig. S4, C to E), we partitioned [$^{13}$C,$^{15}$N]CAPRIN1 into a large preformed FMRP condensed phase (fig. S7 and supplementary text). We acquired carbonyl carbon-amide nitrogen correlation (CON) spectra of [$^{13}$C,$^{15}$N]CAPRIN1 in these condensed phases (fig. S8, A and B) and compared the peak intensities to those from spectra of [$^{13}$C,$^{15}$N]CAPRIN1 in buffer (dilute phase sample) (Fig. 2, B and C). Plotting intensity ratios as a function of sequence, we observed substantial intensity reductions for most CAPRIN1 residues, which we interpret as a combination of dynamic heterogeneous interactions and higher viscosities present in the condensed phases (see supplementary text).

We identified two Arg-rich regions of CAPRIN1 with greater reductions in peak intensities in the co-pFMRP condensed phase than in FMRP, along with small CSPs between these states (Fig. 2, D and E, fig. S8, C and D). We interpret these changes as representing additional dynamic and transient phosphorylation-dependent interactions between CAPRIN1 Arg residues and phosphates in pFMRP. To further examine these interactions, we used a net charge–conserved Arg-to-Lys CAPRIN1 mutant ($Arg^{15}$ → Lys) and found that its binding to pFMRP is much weaker than to the wild type and that it does not phase-separate with pFMRP (fig. S9). Because Lys lacks the π-character of the Arg guanidinium group, Arg π-interactions appear to be important for pFMRP-CAPRIN1 co–phase separation (*9*, *26*).

The two aromatic (Tyr/Phe)–rich regions of CAPRIN1 displayed the largest reductions in peak intensity in both pFMRP and FMRP condensed phases relative to the dilute phase sample (Fig. 2, D and E), consistent with a more general role of interactions of these π-containing regions in protein partitioning into condensates (*9*). The Tyr residues in these regions of CAPRIN1 are known to be phosphorylated in vivo (*22*), which is suggestive of their regulatory function. When we Tyr-phosphorylated CAPRIN1 in vitro (pYCAPRIN1; fig. S3, C and D), we found that pYCAPRIN1 co–phase-separates with FMRP but not with pFMRP (Fig. 3, A and B). To further explore pTyr regulation in aromatic-rich regions, we performed a bioinformatic analysis that revealed

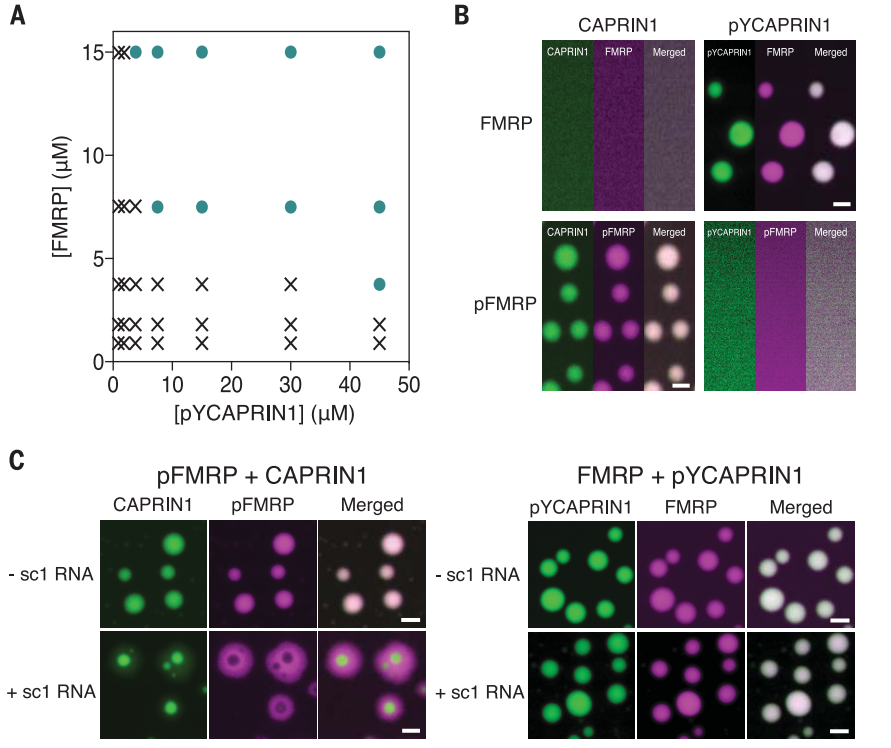


**Fig. 3. Phosphorylation acts as switch for FMRP-CAPRIN1 co–phase separation and a determinant of subcompartmentalization with RNA.** (**A**) Phase diagram for FMRP and pYCAPRIN1 co–phase separation. Teal dots represent conditions of observable droplet formation. (**B**) Fluorescence images showing that phosphorylation of either FMRP-Cy5 or CAPRIN1-FITC promotes co–phase separation, whereas phosphorylation of both proteins, or of neither protein, disfavors co–phase separation. Scale bars, 2 μm. (**C**) Addition of sc1 RNA leads to formation of subcompartments for pFMRP-Cy5–CAPRIN1-FITC condensates (left) but not for pYCAPRIN1-FITC–FMRP-Cy5 condensates (right). Scale bars, 3 μm. Concentrations in (B) and (C): CAPRIN1 and FMRP, 100 μM; pYCAPRIN1 and pFMRP, 30 μM; sc1 RNA, 3 μM.

a strong correlation between numbers of pTyr sites and predicted phase separation (*9*) (fig. S10A). Many known cytoplasmic granule proteins related to mRNA stability, translation, and cellular component organization were identified within the top few percent of highly Tyr-phosphorylated proteins, including CAPRIN1 (fig. S10). Thus, our experimental and bioinformatics results suggest that Tyr phosphorylation could be a general mechanism of regulating translation and mRNA stability by tuning phase separation behavior.

To probe the functional consequences of pFMRP-CAPRIN1 phase behavior, we first produced better models of cytoplasmic RNA bodies by adding RNA into FMRP-CAPRIN1 condensates. Addition of the G-quadruplex–forming sc1 RNA, which has a well-characterized FMRP interaction (*27*), led to multiphasic pFMRP-CAPRIN1 condensates (Fig. 3C, left) reminiscent of partially colocalized FMRP and CAPRIN1 in cellular bodies (*12*). However, we did not observe this multiphasic subcompartmentalization upon addition of RNA to FMRP-pYCAPRIN1 condensates (Fig. 3C, right). To explore the mechanism of condensate subcompartmentalization, we measured protein-RNA binding affinities, because previous reports have shown their importance in facilitating condensate subcompartmentalization (*28*). Using fluorescence polarization, we found that FMRP and CAPRIN1 bind to RNA (either sc1 or polyA$_{38}$) with similar affinities, and that phosphorylation of these proteins results in a similar decrease in RNA affinities (fig. S11). Because pFMRP-CAPRIN1-sc1 RNA forms subcompartments but FMRP-pYCAPRIN1-sc1 RNA does not, subcompartmentalization is not solely due to the differences in RNA binding strengths.

Fluorescence images revealed that fluorescein isothiocyanate (FITC)–labeled CAPRIN1 and sc1 RNA primarily colocalize to the inner phase, whereas Cy5-labeled pFMRP primarily localizes to the outer phase (fig. S12). Higher-resolution microscopy images with deconvolution processing confirmed that these phases are indeed predominantly segregated with sharp transitions in fluorescence intensities (fig. S12E). The dynamic and liquid properties of these coexisting phases were confirmed by fluorescence recovery after photobleaching experiments and observations of liquid-like fusion (fig. S13 and movie S1). Using a previously reported wetting assay (*28*), we found that the hydrophobicity of a recapitulated inner phase of CAPRIN1-RNA differs from that of a recapitulated outer phase of pFMRP-CAPRIN1 (fig. S14). The fluorescence dyes used in our study did not affect phase separation propensity and subcompartmentalization (fig. S15). Therefore, different phosphorylation patterns can act as a switch to form coexisting liquid phases within a condensate that contain distinct biophysical properties.

We next investigated how FMRP-CAPRIN1-RNA condensates affect mRNA deadenylation. Because the deadenylase CNOT7, a catalytic subunit of the CCR4-NOT complex, was shown to be critical for regulating localized translation in neurons (*29*), we used CNOT7 to measure deadenylation rates that can be reflective of translational activity. Adapting a gel-based assay (*5*) that monitors cleavage of a 5′-FITC-labeled polyA$_{38}$ RNA by CNOT7 (fig. S16, A and B), we found that the in vitro deadenylation rate in the presence of pFMRP-CAPRIN1 condensates is ~7.5 times the rate of CNOT7 in buffer (Fig. 4, A and D). In contrast, CNOT7 enzymatic rates in the presence of FMRP-pYCAPRIN1 condensates were comparable to that of buffer control (Fig. 4, A and D, fig. S16, C and D). Thus, different condensate compositions affect in vitro deadenylation rates.

In FMRP-pYCAPRIN1 condensates, CNOT7 and RNA substrate colocalized together (Fig. 4B, bottom) but, surprisingly, in pFMRP-CAPRIN1 multiphasic condensates, CNOT7 and RNA substrate were segregated into different phases (Fig. 4B, top). To explore how a predominant segregation of enzyme and RNA can support faster deadenylation rates, we tested the binding of CNOT7 to individual protein components. Using ITC, we only detected quantifiable CNOT7 binding to CAPRIN1, with ITC data showing two binding regimes (fig. S17). With additional microscopy data, we could assign the initial regime to CAPRIN1 binding to CNOT7 and the latter regime to co–phase separation of CAPRIN1 and CNOT7 (fig. S17A). In vitro deadenylation assays showed that CAPRIN1 binding to CNOT7 is not sufficient to accelerate activity; rather, enzyme activity is enhanced only when CNOT7 is within a CAPRIN1 phase-separated environment (fig. S17A). This suggests that subcompartmentalization produces a CAPRIN1 and CNOT7 inner compartment that accelerates deadenylation rates in a manner similar to CAPRIN1 condensates (Fig. 4D) without appreciably concentrating CNOT7, as the majority remains in the outer compartment. Monitoring the deadenylation reaction over time revealed a size reduction and eventual disappearance of RNA-rich inner compartments, supportive of deadenylation occurring within the inner compartment (Fig. 4C and fig. S18). Together, these results demonstrate that high enzymatic activity does not necessarily imply high relative enzyme concentration and that enzymatic activity can be modulated by CAPRIN1 condensation.

Although phase separation alone can repress translation in vitro without deadenylation, as previously shown for FMRP (*18*), we hypothesize that phase separation can spatially couple the regulation of translation and deadenylation

in cells (*4*, *5*). To test the synergy between translation inhibition and deadenylation, we used a rabbit reticulocyte translation assay and monitored luminescence as a probe for luciferase mRNA translation (*18*) (fig. S19A). We found that condensates with the slowest in vitro translation rates coincide with the fastest deadenylation rates and vice versa (Fig. 4D and figs. S19B and S20). In the presence of pFMRP-CAPRIN1 or CAPRIN1 condensates, in vitro translation was inhibited by a factor of $>10^3$, whereas deadenylation rates were accelerated by a factor of ~7.5. In contrast, pYCAPRIN1 exhibited the fastest translation rates but the slowest deadenylation rates. One potential mechanism by which phase separation can inhibit translation is the simple partitioning of the translational machinery and substrate into different compartments. Although we have not comprehensively screened for protein partitioning, we found that the eukaryotic translation initiation factor 4E (eIF4E) (*30*) is largely excluded from the inner RNA-containing phase of the pFMRP-CAPRIN1 subcompartmentalized condensates, providing evidence for this model (fig. S19C; see supplementary text). Our results demonstrate that different patterns of PTMs and protein compositions of phase-separated compartments can modulate in vitro translation and deadenylation rates in an inversely correlated manner.

Using a simplified model condensate that comprises two IDRs, we found that in vitro deadenylation by CNOT7 can be regulated within CAPRIN1 condensates, possibly because the protein solvent environment modulates CNOT7 activity. For in vitro translation, we infer that inhibition is in part controlled by partitioning of translational machinery into condensates, with partitioning affinities dependent on condensate compositions and PTM states. Mechanistically, condensate compositions can control enzymatic reactions by producing solvent environments that affect binding affinities or allosteric regulation of enzymes, or by segregating reaction components to mitigate product inhibition or to inhibit reactions. The disordered regions of FMRP or CAPRIN1 both contain multiple sites for regulatory phosphorylation, which

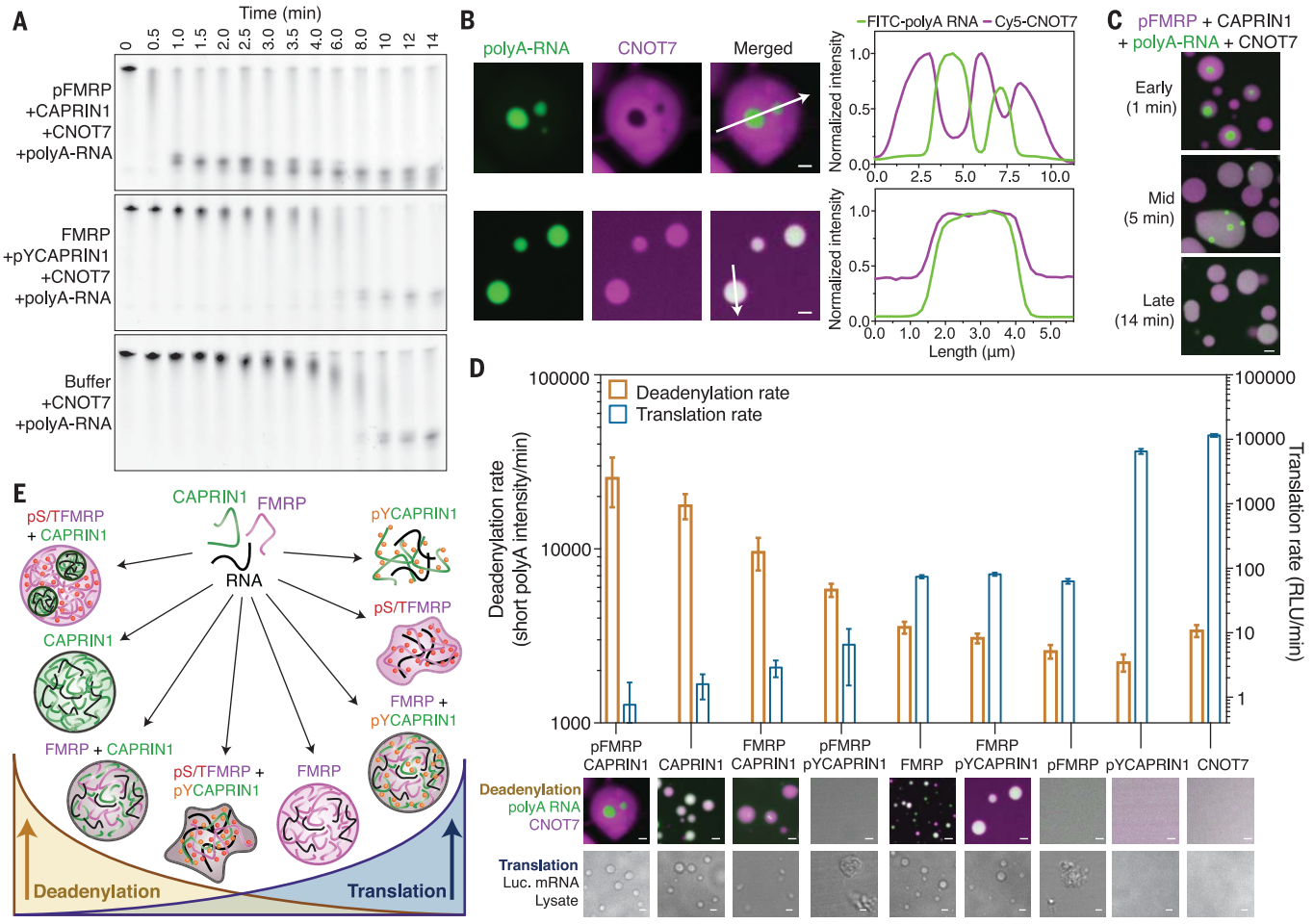


**Fig. 4. In vitro deadenylation and translation rates are modulated by condensate protein compositions and phosphorylation states in an inversely correlated manner.** (**A**) In vitro deadenylation rate is enhanced in subcompartmentalized pFMRP-CAPRIN1-RNA condensates (top) relative to the deadenylation rate in FMRP-pYCAPRIN1-RNA condensates (middle), which is similar to that in buffer (bottom). (**B** and **C**) Fluorescence images of multiphase pFMRP-CAPRIN1-polyA$_{38}$ RNA condensates with CNOT7. (B) Left: CNOT7-Cy5 and 5′FITC-polyA$_{38}$ RNA substrate are largely segregated in pFMRP-CAPRIN1-RNA subcompartmentalized condensates. Cy5-CNOT7 is localized to the outer phase and the majority of 5′FITC-polyA$_{38}$ RNA is localized to the inner phase. For FMRP-pYCAPRIN1-RNA droplets, CNOT7-Cy5 and 5′FITC-polyA$_{38}$ RNA are colocalized. Scale bars, 1.5 μm. Right: Traces of fluorescence intensities through positions denoted by the white arrows in the merged images. (C) RNA enriched in the inner phase decreases in size and disappears over the course of the deadenylation reaction. Scale bar, 2.1 μm. (**D**) In vitro translation and deadenylation rates are modulated in an inversely correlated manner depending on protein composition and phosphorylation status. Representative images of the deadenylation or translation assays are placed below the graph. Error bars represent goodness of fit. (**E**) Different types of Ser/Thr and Tyr phosphorylation patterns control phase behavior (dispersed: no boundary; phase-separated: circular boundaries; gel/aggregate: amorphous boundaries), which coincides with the inversely correlated in vitro deadenylation and translation rates. See supplementary materials for experimental details.

modulates phase behavior in vitro, leading to control of deadenylation and translation activities. Thus, integration of distinct cellular signaling pathways resulting in differential Ser/Thr or Tyr kinase/phosphatase regulation would be predicted to control deadenylation and translation via dynamic remodeling of condensates along a continuum of phase behaviors (Fig. 4E).

## REFERENCES AND NOTES


1. S. F. Banani, H. O. Lee, A. A. Hyman, M. K. Rosen, *Nat. Rev. Mol. Cell Biol.* **18**, 285–298 (2017).
2. Y. Shin, C. P. Brangwynne, *Science* **357**, eaaf4382 (2017).
3. K. Wiederhold, L. A. Passmore, *Biochem. Soc. Trans.* **38**, 1531–1536 (2010).
4. A. C. Goldstrohm, M. Wickens, *Nat. Rev. Mol. Cell Biol.* **9**, 337–344 (2008).
5. M. W. Webster *et al.*, *Mol. Cell* **70**, 1089–1100.e8 (2018).
6. J. R. Buchan, R. Parker, *Mol. Cell* **36**, 932–941 (2009).
7. A. M. Krichevsky, K. S. Kosik, *Neuron* **32**, 683–696 (2001).
8. A. Hubstenberger *et al.*, *Mol. Cell* **68**, 144–157.e5 (2017).
9. R. M. Vernon *et al.*, *eLife* **7**, e31486 (2018).
10. J.-Y. Youn *et al.*, *Mol. Cell* **69**, 517–532.e11 (2018).
11. S. A. Barbee *et al.*, *Neuron* **52**, 997–1009 (2006).
12. R. El Fatimy *et al.*, *PLOS ONE* **7**, e39338 (2012).
13. S. De Rubeis, C. Bagni, *Mol. Cell. Neurosci.* **43**, 43–50 (2010).
14. D.-I. Kao, G. M. Aldridge, I. J. Weiler, W. T. Greenough, *Proc. Natl. Acad. Sci. U.S.A.* **107**, 15601–15606 (2010).
15. S. Solomon *et al.*, *Mol. Cell. Biol.* **27**, 2324–2342 (2007).
16. M. A. Kiebler, G. J. Bassell, *Neuron* **51**, 685–690 (2006).
17. K. Nakayama *et al.*, *eLife* **6**, e29677 (2017).
18. B. Tsang *et al.*, *Proc. Natl. Acad. Sci. U.S.A.* **116**, 4218–4227 (2019).
19. J. Sheu-Gruttadauria, I. J. MacRae, *Cell* **173**, 946–957.e16 (2018).
20. X. Su *et al.*, *Science* **352**, 595–599 (2016).
21. E. R. Towers, J. J. Kelly, R. Sud, J. E. Gale, S. J. Dawson, *J. Cell Sci.* **124**, 1145–1155 (2011).
22. P. V. Hornbeck *et al.*, *Nucleic Acids Res.* **43**, D512–D520 (2015).
23. M. C. Siomi, K. Higashijima, A. Ishizuka, H. Siomi, *Mol. Cell. Biol.* **22**, 8438–8447 (2002).
24. K. A. Burke, A. M. Janke, C. L. Rhine, N. L. Fawzi, *Mol. Cell* **60**, 231–241 (2015).
25. J. P. Brady *et al.*, *Proc. Natl. Acad. Sci. U.S.A.* **114**, E8194–E8203 (2017).
26. T. J. Nott *et al.*, *Mol. Cell* **57**, 936–947 (2015).
27. A. T. Phan *et al.*, *Nat. Struct. Mol. Biol.* **18**, 796–804 (2011).
28. M. Feric *et al.*, *Cell* **165**, 1686–1697 (2016).
29. R. L. McFleder, F. Mansur, J. D. Richter, *Cell Rep.* **20**, 683–696 (2017).
30. J. Pelletier, N. Sonenberg, *Annu. Rev. Biochem.* **88**, 307–335 (2019).


## ACKNOWLEDGMENTS

We thank P. A. Chong and M. Nosella for reading the manuscript with helpful comments; R. Muhandiram and G. Seabrook for assistance with NMR assignment experiments and data; J. Krieger from the Hospital for Sick Children SPARC BioCentre for assistance with mass spectrometry experiments; and G. Wasney from the Hospital for Sick Children Structural and Biophysical Core Facility for helping with ITC and FRET measurements. **Funding:** Supported by a CIHR Banting Postdoctoral Fellowship and a Restracomp Fellowship from the Hospital for Sick Children (T.H.K.), a CIHR Vanier Scholarship (B.T.), and Canadian Institutes for Health Research grant FDN-148375, Natural Sciences and Engineering Research Council of Canada grant RGPIN-2016-06718, and the Canada Research Chairs program (J.D.F.-K.). The 800-Hz NMR spectrometer was funded by the Canada Foundation for Innovation and the NMR Core Facility was supported by the Princess Margaret Cancer Foundation. **Author contributions:** T.H.K., B.T., and J.D.F.-K. conceived the project. T.H.K. and B.T. prepared reagents and performed experiments. T.H.K., B.T., L.E.K., and J.D.F.-K. designed and analyzed the experiments. R.M.V. conducted the bioinformatic analysis. N.S. assisted in conceptualization and analysis of data. T.H.K. and B.T. wrote the manuscript and T.H.K., B.T., R.M.V., N.S., L.E.K., and J.D.F.-K. edited the manuscript. **Competing interests:** Authors declare no competing interests. **Data and materials availability:** All data are available in the main text or the supplementary materials.

## SUPPLEMENTARY MATERIALS

science.sciencemag.org/content/365/6455/825/suppl/DC1
Materials and Methods
Supplementary Text
Figs. S1 to S20
Table S1
Movie S1
References (*31*–*52*)

22 March 2019; accepted 29 July 2019
10.1126/science.aax4240

# Phospho-dependent phase separation of FMRP and CAPRIN1 recapitulates regulation of translation and deadenylation

Tae Hun KimBrian TsangRobert M. VernonNahum SonenbergLewis E. KayJulie D. Forman-Kay

*Science*, 365 (6455), • DOI: 10.1126/science.aax4240

**Keeping RNA processing contained**

Biomolecular condensates that assemble by phase separation are involved in RNA processing. Posttranslational modifications in intrinsically disordered regions of proteins can regulate RNA processing by regulating phase separation. Kim *et al.* used nuclear magnetic resonance spectroscopy to characterize phase separation in a model system comprising the C-terminal disordered regions of the translational regulators FMRP and CAPRIN1 that repress translation by deadenylating mRNA. Interactions between the proteins involve specific sequences in FMRP and CAPRIN1, and the propensity for mRNA to partition into the condensates depends on the phosphorylation patterns in the disordered regions. This mechanism integrates signaling pathways with the regulation of RNA processing.

*Science*, this issue p. 825